Appl. Phys. B 88, 205–209 (2007)
DOI: 10.1007/s00340-007-2708-5

Applied Physics B
Lasers and Optics

A. MAJKIĆ[1,✉]
G. POBERAJ[1]
R. DEGL'INNOCENTI[1]
M. DÖBELI[2]
P. GÜNTER[1]

Cr:LiSrAlF$_6$ channel waveguides as broadband fluorescence sources

[1] Nonlinear Optics Laboratory, Institute of Quantum Electronics, ETH Zürich, 8093 Zürich, Switzerland
[2] Paul Scherrer Institute, c/o Institute for Particle Physics, ETH Zürich, 8093 Zürich, Switzerland

Received: 6 February 2007/Revised version: 18 May 2007
Published online: 26 June 2007 •

ABSTRACT We report on the production and fluorescence of active channel waveguides in Cr:LiSrAlF$_6$. We have produced $\sim 10\,\mu$m wide and 5 μm high channel waveguides by He^+ ion implantation, lithographic patterning and subsequent Ar^+ ion sputtering. Diode-pumped waveguides emitted 13 μW of fluorescence light with a spectrum ranging from 760 nm to 900 nm at a pump power of 165 mW and a pump wavelength of 660 nm. The compact and cheap optical pump source is a main advantage of this fluorescence material. This makes Cr:LiSrAlF$_6$ channel waveguides a suitable candidate for a broadband fluorescence source in low-coherence interferometry and other applications in the near-infrared wavelength range.

PACS 42.70.Hj; 42.79.Gn; 42.30.Wb

1 Introduction

Cr:LiSrAlF$_6$ (Cr:LiSAF) is an interesting fluorescent material characterised by a wide emission bandwidth in a wavelength range of 750–930 nm, similar to that of Ti:sapphire, which makes it useful for tuneable laser action or ultra short pulse operation. Similarly as Ti:sapphire [1], this material may also be used as a broadband fluorescence source in optical low coherence interferometry and particularly in optical coherence tomography (OCT) [2]. However, the broadband light source based on Cr:LiSAF could be cheaper and more compact since its wide absorption band in the 640–680 nm range [3] permits direct optical pumping with commercially available red laser diodes. The material's low peak emission cross section requires a high pump power density for efficient fluorescence or cw lasing. However, high heat generation density leads to enhanced thermal quenching [4, 5], which is difficult to counteract in a bulk crystal, since the material thermal conductivity is rather low [6]. Both high optical pump power density and efficient heat removal can be provided by confining the light in a waveguide. In addition, the output light of channel waveguides can be more effectively coupled into a single mode fibre, as required for OCT applications. Recently, extensive research of broadband fluorescence sources in waveguide geometry has been carried out using Ti:sapphire. Active planar waveguides [7], active channel waveguides [8, 9] as well as waveguide lasers [10, 11] have already been presented. In the case of fluorides, research of waveguides in most common fluoride materials is reviewed in [12]. For Cr:LiSAF, only the fabrication of planar waveguides by ion implantation was reported [13]. In this paper, we report on the extensive work that has been recently carried out in our laboratory, with the goal of developing a compact Cr:LiSAF waveguide fluorescence source and ultimately a waveguide laser.

This paper is structured as follows. The fabrication of planar and channel waveguides is briefly described in Sect. 2. A detailed optical characterisation of the obtained waveguides is covered in Sect. 3. Section 3.1 shows the results of the measurements of the propagation losses and induced refractive index change. The fluorescence emission spectral and spatial properties, the emitted fluorescence power and the optical amplification are presented and discussed in Sect. 3.2. Conclusions are drawn in Sect. 4.

2 Waveguide fabrication

For producing Cr:LiSAF channel optical waveguides we used a three-step process based on light ion implantation, lithographic patterning and Ar^+ sputtering. In the past, we have already demonstrated the suitability of this method for the waveguide fabrication in various inorganic [14–16] and organic [17] nonlinear optical crystals. In our experiments we used 5.5% doped optically polished Cr:LiSAF crystals. High doping was chosen in order to increase the output power and minimize the propagation losses by keeping the waveguides short. Implantations were performed with 2.4 MeV He^+ ions, giving planar waveguides with a thickness of $\sim 6.5\,\mu$m. Ion fluencies ranging from 2 to 15×10^{15} ions/cm^2 were used, with an average current density of 0.2 μA/cm^2. Implantations were carried out at 100 K, with the ion beam direction slightly off from the orthogonal to the crystal surface in order to avoid channelling effects. Both *a*-cut and *c*-cut crystals (*c*-crystal axis || and $\perp$ to the implanted surface, respectively) were implanted.

In most of the *a*-cut crystals the surface became brittle upon implantation. As shown in Fig. 1, striations [13], larger cracks, split-off islands and peeling-off of the surface layer

✉ Fax: +41-44-633-1056, E-mail: majkic@phys.ethz.ch

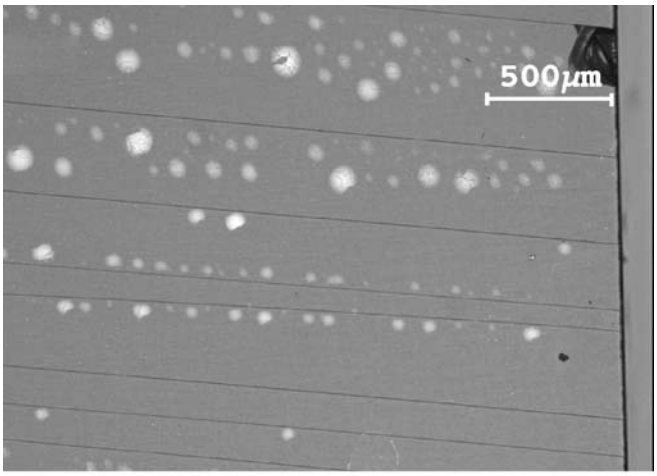

a

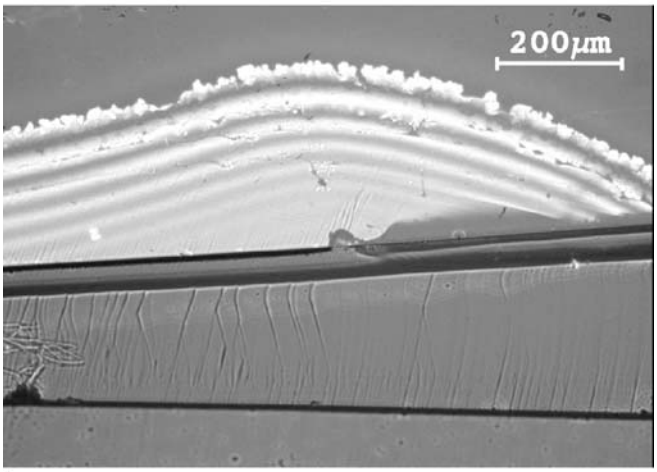

b

FIGURE 1 Optical micrograph of an a-cut crystal after the implantation with 2.4 MeV He^+ ions. (**a**) Striations and split-off islands are visible. Fluence was 0.75×10^{16} ions/cm^2. (**b**) A larger crack runs horizontally through the photo. A layer peeled off, starting from the crack. Fluence was 1.5×10^{16} ions/cm^2

developed with the growing implantation fluence. The thickness of the peeled-off layer did not always coincide with the implantation depth, but was in some cases ~ 2.5 times larger. No surface cracking was observed in the *c*-cut implanted crystals. Therefore, our research was focused on the development of waveguides in the *c*-cut crystals. Since the emission cross-section for the π- transition (E||c) is ~ 2.5 times higher than for the σ- transition (E$\perp$c), focus was put on the TM waveguide modes.

Channel waveguides were fabricated out of planar waveguides by photolithographic patterning and subsequent Ar^+ sputtering. Since waveguide modes shift toward the optical barrier (see Sect. 3.1), a rib height close to the waveguide thickness is needed for complete lateral confinement of the propagating light. The achievable height of the smooth sputtered ribs was 4–5 μm, thus limiting the suitable planar waveguide thickness to ~ 5 μm. We thinned the already available implanted planar waveguides from 6.5 μm down to ~ 5 μm by Ar^+ sputtering of the unmasked crystals. Essentially the same planar waveguides could also be fabricated directly by implanting the bulk crystals with ~ 1.9 MeV He^+ ions. As

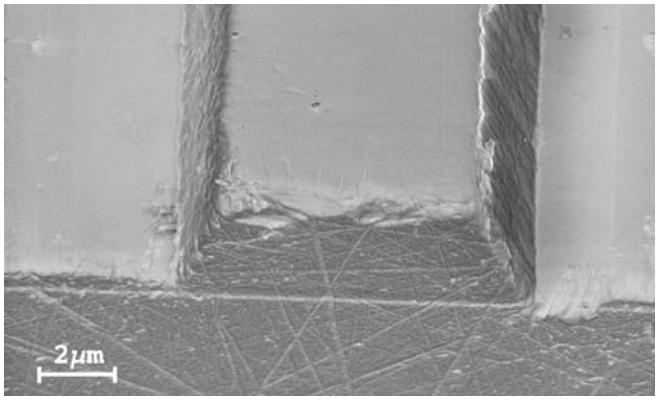

FIGURE 2 SEM image of the fabricated rib structure. The He^+ stopping region is clearly recognizable as a sharp groove, separating the rib from the bulk. The waveguide cross section is trapezoidal with the width at the base $w \sim 11$ μm, width on top $d \sim 9$ μm and height $h \sim 5$ μm

a first step of the rib fabrication, a 5.3 μm thick photoresist (PR) layer (Clariant AZ 4533) was spin-coated on top of the implanted crystal surface. Photoresist stripes of 11 μm width were then formed by standard photolithography and hardened with a 30 min hardbake at 115 °C. After that, the PR pattern was transferred down to the Cr:LiSAF planar waveguide by Ar^+ sputtering (Oxford Plasmalab 80, RF power 300 W) and the 5.0 μm high ribs were finally fabricated. The sputter rates of the Cr:LiSAF and the PR mask were 3.9 nm/min and 1.9 nm/min, respectively. The obtained structures were investigated with a profilometer and a scanning electron microscope (SEM). In Fig. 2 an SEM image of the fabricated rib waveguide with a polished end facet is shown. The He^+ stopping region is clearly seen as a sharp groove, separating the rib from the bulk material.

3 Optical characterisation

3.1 *Refractive index profile and propagation losses*

By TM dark mode spectroscopy using prism coupling we could determine the refractive index profile n_e in the surface region of the crystal. The calculation method is presented in more detail in [18]. Figure 3 shows a reconstructed refractive index profile that best matches the measured data, together with the mode curve of the measured and calculated waveguide modes. The FWHM of the calculated barrier is ~ 0.5 μm, which is in agreement with the SRIM-2003 (stopping and range of ions in matter [19]) simulation. Comparison between the calculated index profile and the simulation of the implantation damage implies that the electronic energy loss (EEL) of He^+ ions shapes the nonuniform index profile in the wave-guiding layer. The EEL reaches its maximum at ~ 3.5 μm and drops steeply afterwards. The nuclear energy loss (NEL) occurs only at the end of the ion track and gives shape to the low-index optical barrier. In-between, there is a window of minimal combined loss (EEL and NEL) that results in a smaller index decrease at ~ 5.5 μm. Consequently, the centre of the waveguide modes shifts toward the barrier (see Fig. 5).

In order to optimize the performance of a potential waveguide laser or a broadband fluorescence source, the propagation losses at both the pump wavelength and especially the

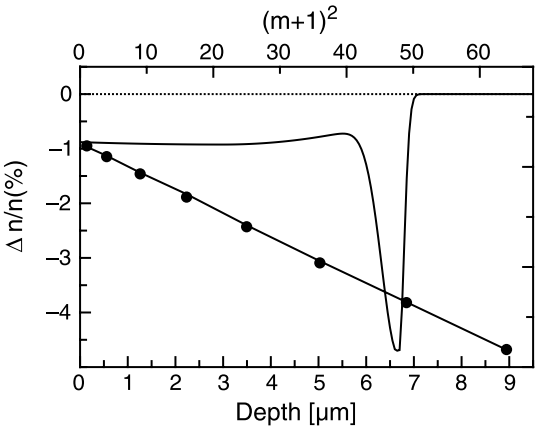

FIGURE 3 Refractive index profile for an implantation with 5×10^{15} ions/cm^2, measured at 633 nm. The *data points* represent the measured TM dark mode positions and the *solid curve* through them gives the theoretical mode positions corresponding to the shown fitted profile

emission wavelength should be as low as possible. Measurements of the planar waveguide propagation losses at the near-infrared (NIR) emission wavelength of 830 nm (close to the max. of fluorescence, see below) were performed using the end-coupling configuration. A tuneable Cr:LiSAF laser (IR-Point, Rainbow Photonics) was employed as the source of the probe beam. The transmitted waveguide output was selected with the aperture and measured with a silicon power meter. Two cylindrical lenses were used to focus the collimated beam in one plane and couple it into- and out of the planar waveguide. The lowest propagation losses of 9 ± 1 dB/cm (TM polarisation, assuming a coupling efficiency of 80%) were measured in the waveguides implanted with a fluence of 5×10^{15} ions/cm^2. Relatively high losses are attributed to the absorption due to implantation-generated colour centres and to the tunnelling through the barrier. In order to reduce the losses due to absorption, the pulsed laser annealing (PLA) technique was suggested in [13]. However, the PLA performed similarly as in [13] did not reduce the losses. It is believed that the ultraviolet light penetrated the crystal far beyond the wave-guiding layer and accordingly annealed the barrier as well. Alternatively, thermal annealing was performed for up to 10 h at $\sim 210\,^\circ$C. The measured losses decreased for $\sim 5\%$, which is still within the experimental error of the loss measurement.

Channel waveguides fabricated by etching techniques usually suffer from additional losses with respect to the planar waveguides due to additional scattering on the waveguide sidewalls. The attenuation of the light propagating in the fabricated rib waveguides was measured by a similar end-coupling setup, in which the microscope objectives of magnification $10\times$ were used to couple the light into- and out of the rib waveguides. The lowest value of the measured losses in a 2.0 mm long crystal for TM polarised light at $\lambda = 830$ nm was 10 ± 2.5 dB/cm, assuming a coupling efficiency of 80%. Because of strong tunnelling, the electric field of the light propagating in the waveguide extended significantly beyond the barrier. Comparison of the propagation losses in planar and channel waveguides suggests that surface scattering could have only a minor contribution (of < 1 dB/cm) to the overall propagation losses. Two major sources of losses were tunnelling through the optical barrier and absorption caused by the colour centres. According to the numerical simulation of the light propagating in the rib waveguide, the tunnelling and the absorption had similar contributions to the light attenuation in the waveguide.

3.2 *Fluorescence emission characteristics*

The spectral, spatial and power characteristics of the fluorescence light emitted by the optically pumped channel waveguides were investigated. A single transversal mode red laser diode (Opnext HL6526FM, max. 165 mW at 660 nm) was used as the optical pump source. The fluorescence emission from the exit facet of the waveguide was imaged by a microscope objective onto the spectrometer, CCD camera and silicon power meter, respectively. A long-pass filter was used to remove the residual pump radiation.

Figure 4 shows the measured spectra of the fluorescence light emitted from the waveguide and from the bulk crystal. The spectra differ only slightly, which suggests that the local environment of the active Cr^{3+} ions remained mostly unaltered after the implantation. The spectrum width in the case of the waveguide was 75 nm FWHM, compared to 85 nm FWHM in the bulk material. The spectral distribution is narrower on the long wavelength side and the spectrum peak of the waveguide output is shifted for 7 to 803 nm. Both effects can be attributed to the comparatively higher tunnelling losses on the longer-wavelength side. The intensity profile of the fluorescence emitted from the waveguide is shown in Fig. 5. The measured intensity profile is symmetrical and strongly confined in the horizontal direction as a consequence of the 5 μm deep etching. The asymmetry in the vertical plane ($\perp$ to the implanted surface) is attributed to the nonuniform refractive index within the waveguide and to the leakage of light through the optical barrier into the bulk material.

The output power of the fluorescence emission as a function of the input optical pump (P_p) power is shown in Fig. 6. The maximal measured fluorescence output power was around 13 μW at 165 mW input power. The crystal's base surface was held at 6 °C. According to our estimation, the temperature in the front part of the waveguide rose to 60–100 °C for $P_\mathrm{p} = 100$ mW. Therefore, we suppose that strong thermal quenching occurred and suppressed the emission at higher

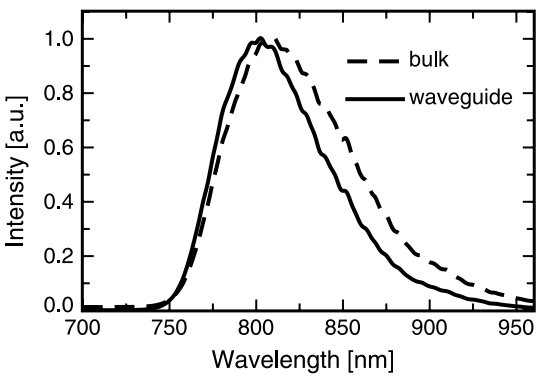

FIGURE 4 Measured spectrum of the fluorescence light emitted out of the waveguide (*solid line*) and the underlying bulk material (*dashed line*). The fluorescence spectrum of the waveguide remains predominantly unchanged

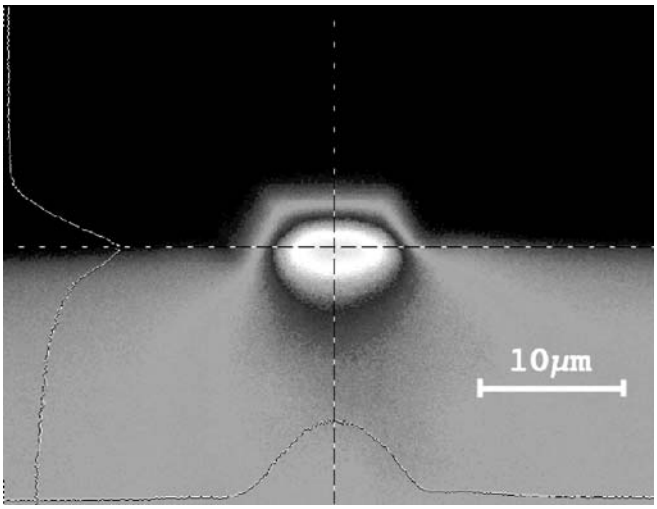

FIGURE 5 Fluorescence emission profile measured at the exit of the channel waveguide. Waveguide dimensions as in Fig. 3

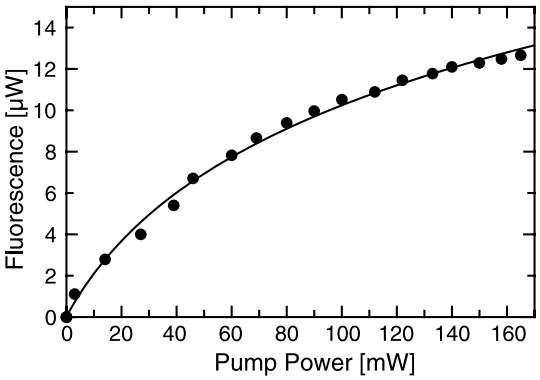

FIGURE 6 Emitted fluorescence power as a function of the input optical pump power. The *line* connecting the measurement points is a guide to the eye. The actual in-coupled pump power is $\sim 0.7\times$ input power. Dimensions of the waveguide: cross-section as in Fig. 3, length is 2.0 mm

input powers. This would explain why the slope efficiency decreased from $\sim 15 \times 10^{-5}$ to $\sim 4 \times 10^{-5}$ with increasing input power. Polarisation ratio of the emitted fluorescence was $I_c : I_a \approx 2.4 : 1$, which is in agreement with the ratio of the corresponding emission cross-sections in a bulk crystal [3].

Additionally, the NIR probe beam was coupled simultaneously with the pump beam into the waveguide and the optical amplification of the NIR light was measured. The NIR power before the first microscope objective was 2.1 mW, the out-coupled power was 0.82 mW, which gave a propagation loss of 10.3 dB/cm for that particular waveguide. The rise of the NIR output with increasing optical pump is shown in Fig. 7. The out-coming NIR increased nearly proportionally to the input optical pump until $P_\mathrm{p} \sim 70$ mW, after which it remained constant, within the measurement error. We simulated NIR amplification along the waveguide with a simplified one-dimensional numerical model using the laser rate equations. The measurement data were in good agreement with the model for the product $n_t \times \tau_\mathrm{f}$ being approximately 20–25 times smaller than the $n_{t0} \times \tau_{\mathrm{f}0}$ of the bulk material, where, n_t is the density and τ_f is the fluorescence lifetime of the active Cr^{3+} ions in the waveguide, respectively. We believe that due to a temperature increase within the waveguide the major

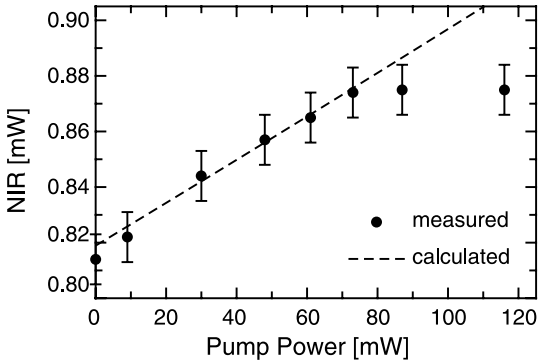

FIGURE 7 Measured and simulated transmitted NIR light as a function of input pump power. The waveguide is the same as in Fig. 6

contribution to the drop of $n_t \times \tau_\mathrm{f}$ came from a smaller fluorescence lifetime due to thermal quenching, at least at higher optical pump powers.

4 Conclusion

Cr:LiSAF channel waveguides have been fabricated by He^+ implantation and Ar^+sputtering. The waveguides supported NIR optical mode propagation with moderate propagation losses. The two major sources of propagation losses were found to be tunnelling through the optical barrier and absorption due to colour centres. Losses in the channel waveguides did not increase significantly with respect to the ones in planar waveguides due to the smooth rib surface of the channel waveguides. The fluorescence emitted from the optically pumped waveguides was spatially well confined and had a wide spectrum ranging from 760 nm to 900 nm. Therefore, we expect that such devices could be considered as the fluorescence source in low-coherence interferometry where high longitudinal resolution is needed. The fluorescence output power in these proof-of-concept experiments was up to 13 μW at 165 mW of pump power. The output power could be further increased by optimising the optical barrier and by a more efficient annealing. Thermal quenching was the most probable cause that limited the output power. Attaching a clad waveguide directly to a heat sink could significantly diminish thermal quenching and allow a further increase of the emitted fluorescence output power.

ACKNOWLEDGEMENTS The authors thank J. Hajfler for polishing the crystals. This work was partially supported by the Swiss Innovation Promotion Agency (KTI Nr. 4753.1 SUS-NM).

REFERENCES

1 A.M. Kowalevicz, T. Ko, I. Hartl, J.G. Fujimoto, M. Pollnau, R.P. Salathé, Opt. Express **10**, 349 (2002)
2 D. Huang, E.A. Swanson, C.P. Lin, J.S. Schuman, W.G. Stinson, W. Chang, M.R. Hee, T. Flotte, K. Gregory, C.A. Puliafito, J.G. Fujimoto, Science **254**, 1178 (1991)
3 S.A. Payne, L.L. Chase, L.K. Smith, W.L. Kway, H.W. Newkirk, J. Appl. Phys. **66**, 1051 (1989)
4 M. Stalder, M. Bass, B. H T. Chai, J. Opt. Soc. Am. B **9**, 2271 (1992)
5 S. Uemura, K. Miyazaki, Japan. J. Appl. Phys. **36**, 4312 (1997)
6 S.A. Payne, L.K. Smith, R.J. Beach, B.H.T. Chai, J.H. Tassano, L.D. DeLoach, W.L. Kway, R.W. Solarz, W.F. Krupke, Appl. Opt. **33**, 5526 (1994)

7 M. Pollnau, R.P. Salathé, T. Bhutta, D.P. Shepherd, R.W. Eason, Opt. Lett. **26**, 283 (2001)
8 C. Grivas, T.C. May-Smith, D.P. Shepherd, R.W. Eason, M. Pollnau, M. Jelinek, Appl. Phys. A **79**, 1195 (2004)
9 A. Cruteanu, M. Pollnau, G. Jänchen, C. Hibert, P. Hoffmann, R.P. Salathé, R.W. Eason, C. Grivas, D.P. Shepherd, Appl. Phys. B **75**, 15 (2002)
10 L.M.B. Hickey, V. Apostolopoulos, R.W. Eason, J.S. Wilkinson, A.A. Anderson, J. Opt. Soc. Am. B **21**, 1452 (2004)
11 C. Grivas, D.P. Shepherd, T.C. May-Smith, R.W. Eason, M. Pollnau, Opt. Express **13**, 210 (2005)
12 R. Burkhalter, I. Dohnke, J. Hulliger, Prog. Cryst. Growth. Charact. Mater. **42**, 1 (2001)
13 P.J. Chandler, X. Huang, P.D. Townsend, N. Hamelin, Y.T. Chow, Nucl. Instrum. Methods Phys. Res. B **127**/**128**, 528 (1997)
14 D. Fluck, P. Günter, IEEE J. Sel. Top. Quantum Electron. **6**, 122 (2000)
15 R. Degl'Innocenti, A. Guarino, G. Poberaj, P. Günter, Appl. Phys. Lett. **89**, 041 103 (2006)
16 A. Guarino, M. Jazbinšek, C. Herzog, R. Degli'Innocenti, G. Poberaj, P. Günter, Opt. Express **14**, 2344 (2006)
17 L. Mutter, A. Guarino, M. Jazbinšek, M. Zgonik, M. Döbeli, P. Günter, Opt. Express **15**, 629 (2007)
18 P.D. Townsend, P.J. Chandler, L. Zhang, *Optical Effects of Ion Implantation* (Cambridge University, Cambridge, 1994)
19 J.F. Ziegler, J.P. Biersack, U. Littmark, *The Stopping and Range of Ions in Solids* (Pergamon, New York, 1985)